analytical chemistry

Article

pubs.acs.org/ac

Multiwavelength Fluorescence Otoscope for Video-Rate Chemical Imaging of Middle Ear Pathology

Tulio A. Valdez,*[,†,‡,#] Rishikesh Pandey,[§,#] Nicolas Spegazzini,[§] Kaitlyn Longo,[†,‡] Corrie Roehm,[†] Ramachandra R. Dasari,[§] and Ishan Barman*[,∥,⊥]

[†]Otolaryngology - Head and Neck Surgery, University of Connecticut, Storrs, Connecticut 06269, United States
[‡]Otolaryngology - Head and Neck Surgery, Connecticut Children's Medical Center, Hartford, Connecticut 06106, United States
[§]Laser Biomedical Research Center, Massachusetts Institute of Technology, Cambridge, Massachusetts 02139, United States
[∥]Department of Mechanical Engineering, Johns Hopkins University, Baltimore, Maryland 21218, United States
[⊥]Department of Oncology, Johns Hopkins University, Baltimore, Maryland 21287, United States

ABSTRACT: A common motif in otolaryngology is the lack of certainty regarding diagnosis for middle ear conditions, resulting in many patients being overtreated under the worst-case assumption. Although pneumatic otoscopy and adjunctive tests offer additional information, white light otoscopy has been the main tool for diagnosis of external auditory canal and middle ear pathologies for over a century. In middle ear pathologies, the inability to avail high-resolution structural and/or molecular imaging is particularly glaring, leading to a complicated and erratic decision analysis. Here, we propose a novel multiwavelength fluorescence-based video-rate imaging strategy that combines readily available optical elements and software components to create a novel otoscopic device. This modified otoscope enables low-cost, detailed and objective diagnosis of common middle ear pathological conditions. Using the detection of congenital cholesteatoma as a specific example, we demonstrate the feasibility of fluorescence imaging to differentiate this proliferative lesion from uninvolved middle ear tissue based on the characteristic autofluorescence signals. Availability of real-time, wide-field chemical information should enable more complete removal of cholesteatoma, allowing for better hearing preservation and substantially reducing the well-documented risks, costs and psychological effects of repeated surgical procedures.

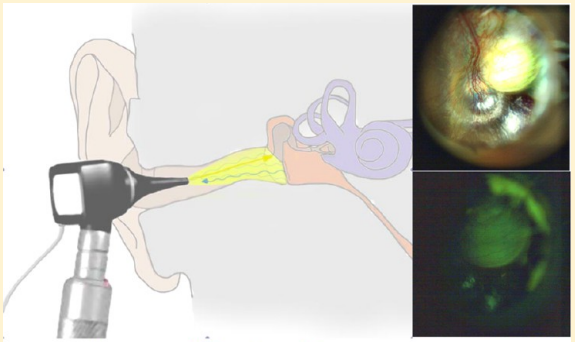

Despite the high incidence of clinical visits that pertain to middle ear pathologies, our ability to make a rapid and accurate diagnosis of these conditions has not improved considerably over the years. Reliable diagnosis of middle ear conditions remains challenging, and the accuracy of currently available methods is limited.[1−3] At present, standard ear evaluations include interpretation of the clinical history combined with otologic examinations for visual inspection. Otoscopic examinations rely primarily on the white light otoscope reflection utilizing a device that has undergone relatively few modifications since first described in the 1860s. Although pneumatic otoscopy and adjunctive tests offer additional information, white light otoscopy has proved to be the diagnostic tool of choice for well over a century. White light otosocopy has been routinely used by both primary care physicians and specialists for evaluation of middle ear pathologies ranging from highly proliferative and destructive conditions such as cholesteatomas to acute otitis media (AOM) and tympanic membrane perforations.

As a case in point, cholesteatomas are expansive and destructive lesions characterized by migration of keratinized hyperproliferative squamous epithelium with a fibrous stroma that can occur in the middle ear and mastoid cavity.[4] Under the invading epithelial layer, ossicular and bony erosion occur with potential complications ranging from otomastoiditis and facial nerve paralysis to intracranial meningitis and perilymphatic fistula.[5] While the underlying pathophysiology remains a subject of much debate, these lesions do not metastatize and are not genetically unstable. Nevertheless, they represent a surgical condition and resolution of the disease process can only occur after complete externalization or removal of the lesion.[4,6] The objective of cholesteatoma surgery is to obtain a dry safe ear; however, this may require multiple surgical procedures, creating significant burden both economically and in the quality of life on those affected by this disease.[7] Consequently, it is imperative to develop new tools that can provide near real-time, reliable and low-cost diagnosis of cholesteatoma and facilitate its complete removal during

Received: August 14, 2014
Accepted: September 16, 2014
Published: September 16, 2014

   dx.doi.org/10.1021/ac5030232 | *Anal. Chem.* 2014, 86, 10454−10460

surgery. It is envisioned that such tools would permit early and robust detection of a wide variety of ear pathologies while also providing specific molecular insight into the onset and progression of the disease states.

Clearly, such an in vivo diagnostic approach should allow direct visualization through the tympanic membrane, thereby allowing clinicians to determine transtympanic middle ear pathologies. This guiding principle underscores the importance of having a photonic/endoscopic method that can adopt the general architecture of the otoscope, which successfully achieves this functional requirement (presumably one of the principal factors behind its longstanding usage) and that can be adapted to an otoendoscope, which can be used at the time of the surgical procedure. However, classical otoscopic evaluation suffers from observer variability and provides limited insight into a disease's defining biochemistry. Molecular methods, in contrast, provide objective biomarkers for diagnoses, may permit disease detection prior to morphologic manifestations and, most importantly, can provide patient stratifications for more effective therapy. In this milieu, spectroscopic imaging offers a novel approach to bridge the chemical and morphologic domains.[8,9] Driven by the promise of nondestructive and nonionizing measurements that can provide observer-invariant diagnosis, molecular spectroscopy has received considerable contemporary attention for diagnosis of diabetes[10] and cancers in various organs including breast,[11] skin[12] and bladder.[13]

The chemical imaging of middle ear pathologies, however, is largely unexplored and no method exists to reproduce or exceed otoscopic capabilities. Although there are a few published reports in the broader domain of neoplasia detection in otorhinolaryngology,[14−16] relatively less attention has been focused on middle ear evaluation. The first spectroscopic findings of significance by Sikora, Richards-Kortum and co-workers highlight the potential of optical imaging with a high-resolution microendoscope but requires the application of exogenous imaging agents (proflavine).[17] We have, on the other hand, suspected that exploiting the endogenous biochemical contrast may provide sufficient information to aid the process of middle ear disease diagnosis and guidance for excision of cholesteatoma.

In this article, we propose a novel diagnostic strategy based on acquisition of autofluorescence signatures that reflect the tissue composition. We have developed a multiwavelength, video-rate fluorescence-based imaging device to detect the underlying biochemical changes of middle ear pathology. Critically, our device design used the existing otoscope architecture as the platform and incorporates readily available optical components as a self-contained, modular ("add-on") feature, which can also be implemented in an otoendoscope. This ensures the ability to make concomitant fluorescence measurements and conventional otoscopic evaluation and substantially reduces registration errors that are frequently observed in similar devices. Though our approach is generally applicable to broad-spectrum evaluation of middle ear pathology, we demonstrate its utility here using cholesteatoma as the paradigm. The proposed device provides a novel mechanism to acquire real-time intraoperative images of the tissue epithelium thereby optimizing the value of the initial procedure and reducing the necessity for a revision surgery for residual disease.

MATERIALS AND METHODS

Design and Construction of the Fluorescence Otoscope. The multiwavelength fluorescence otoscope was designed to acquire autofluorescence signals from the middle ear, the tympanic membrane and transtympanic membrane space (Figure 1). Harnessing the multiwavelength measurements would not only enable the fluorescence-based estimation of multiple endogenous tissue chromophores (prominently collagen, NADH, elastin, tryptophan, FAD and porphyrins) but would also provide the ability to explore differences in tissue absorption and scattering. The latter is of value in understanding the optical penetration depth, which would provide a valuable parameter for identification of fluid presence in diagnosis of AOM.

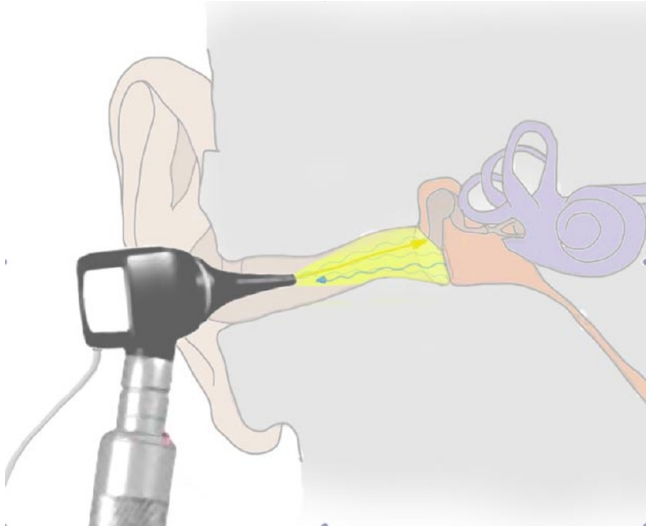

Figure 1. Schematic diagram of fluorescence otoscopy of the middle ear. Our design incorporates regular ear speculums that allow adequate maneuvering in the external auditory canal.

Here, two specific wavelengths were chosen for the proof-of-concept experiments, i.e., 405 and 450 nm based on their relative ability to excite these fluorophores. Specifically, the former is expected to serve as principal indicator of collagen[18] as well as the redox ratio,[19] which is defined as the ratio of the FAD fluorescence to the sum of FAD and NADH signals; whereas the latter would provide a baseline signal corresponding to the nonspecific tissue autofluorescence background (and presumably the tail end of the some of the aforementioned autofluorescence signals). This is based on previous findings that observed a strong correlation between the increase in tissue metabolic activity associated with the progression of epithelial neoplasm and an increase in NADH fluorescence.[20−23] The latter would result in a corresponding decrease in the redox ratio.

The multiwavelength fluorescence otoscope module is based on the Welch Allyn Macroview otoscope head (Figure 2). The use of this otoscope head allows for 30% greater magnification than a traditional otoscope with the ability to adjust focus for variable ear canal length. The excitation source of this prototype consists of two high power light emitting diodes (LEDs), visible (LZ4-00MD00, Mouser Electronics, Mansfield, TX) and UV (LZ1-000A00, Mouser Electronics, Mansfield, TX) LEDs. The visible LED source consists of four LEDs of different colors, i.e., red (625 nm), green (523 nm), blue (450

dx.doi.org/10.1021/ac5030232 | Anal. Chem. 2014, 86, 10454−10460

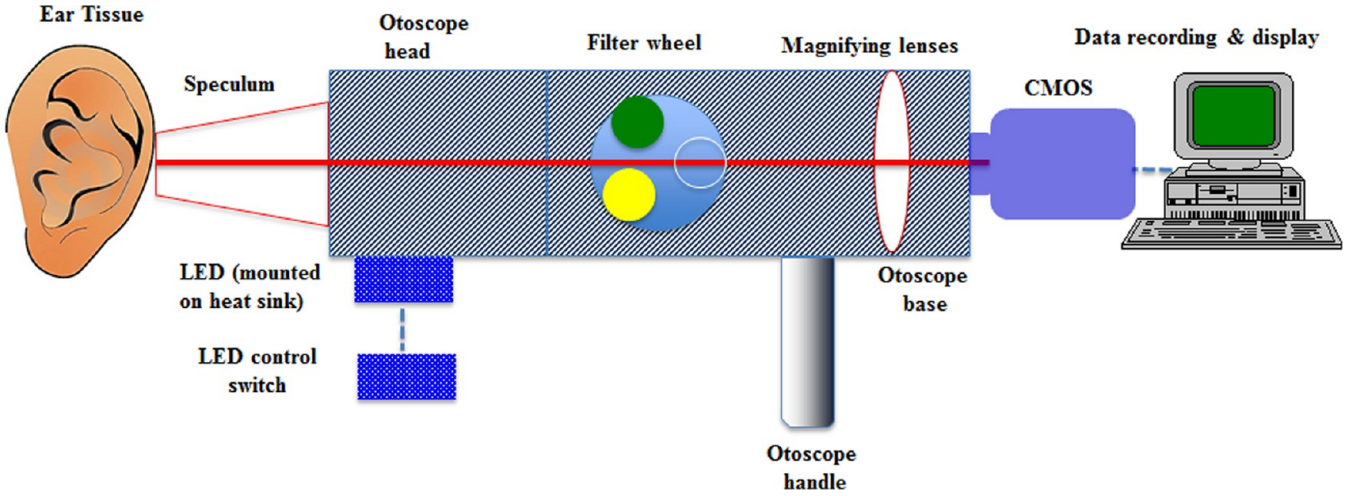

Figure 2. Block diagram of the fluorescence otoscope prototype.

nm) and white, which can be individually operated independently. The UV (400–405 nm) LED source has a single LED. Both the LED sources are mounted on two individual heat sinks (located just beneath the Welch Allyn otoscope head) that are designed to hold LEDs in a stable enclosure using a spring locking mechanism for maximum efficiency. Light from the heat sink cavity was directed into the ear through the Welch Allyn otoscope head. The light emitted was then passed through emission filters mounted on the custom-built filter wheel. An aluminum optical insert was designed to secure the filter wheel into the base of the frame. The filter wheel comprises of three 1″ diameter filter slots. A single filter compartment was left empty to permit traditional white light otoscopic evaluation. Each specific excitation–emission modality could be swapped into the detection module serially. A 425 nm long pass filter was employed for 405 nm excitation, whereas a 500 nm long pass filter was used in conjunction with the 450 nm LED source. The bright field and fluorescence images were recorded on a CMOS camera (DCC1645C, 1280 × 1024 square pixels of 3.6 μm, Thorlabs Inc.) mounted on the otoscope frame, with the user-defined capability of recording either single-shot images or videos at up to 25 frames per second.

Data Acquisition from Human Subjects. To demonstrate the utility of the device through proof-of-principle experiments, we conducted human subject studies at the Connecticut Children's Medical Center. The study protocol was approved by the hospital's institutional review board (IRB) and participants provided informed consent prior to their participation. Inclusion was limited to patients undergoing an otologic surgical procedure under general anesthesia. In this pilot study, we tested 11 patients suffering from cholesteatoma (3, congenital; 8, acquired) with their contralateral normal ears serving as study controls. Additionally, several healthy human subjects were tested to test for potential variations from the normal controls.

After initial visual inspection, any impeding cerumen or debris were removed to provide an optimal view of the tympanic membrane. A video otoscope using a 2.5 or 4 mm speculum was inserted into the external auditory canal until the tympanic membrane was adequately identified under standard white light inspection. Once adequate identification of the normal anatomic landmarks of the tympanic membrane and middle ear was established, fluorescence image acquisition was initiated. As per the established study protocol, the 405 nm excitation source was first used to acquire the fluorescence image using the 425 nm long pass filter. Subsequently, the 450 nm excitation source was employed to acquire the fluorescence image (with a 500 nm emission filter). The digital images were saved in bitmap (bmp) format and videos were stored in avi format. Image acquisition was performed from normal ears and congenital cholesteatomas. The relevant clinical information (pathophysiological condition and spectral dataset) with donor information removed was submitted for analysis and interpretation. Spatial intensity maps and contrast enhancement was pursued in the Matlab 8.3 environment (The MathWorks Inc., Natick, MA). In addition, contrast enhancement of the color images is done by transforming the image to a color space, which has image intensity as one of its components. Singular value decomposition (SVD)-based denoising was performed in conjunction with contrast-limited adaptive histogram equalization (CLAHE) operation.

Following identification and image acquisition, the cholesteatoma specimens were surgically removed and sent for histological processing. Specifically, the samples were fixed in 10% neutral buffered formalin and paraffin-embedded. Sections were subsequently cut for hematoxylin and eosin (H&E) staining prior to microscopic examination by a board-certified pathologist.

RESULTS

As alluded to in the Materials and Methods section, white light illumination was employed to adequately identify the anatomic landmarks in the middle ear, as per the standard operating procedure of a clinical examination. This allows for adequate detailing of the tympanic membrane anatomy and vasculature. Additionally, it also offers adequate transtympanic illumination of the promontory in the middle ear, which is visible due to the translucent nature of the tympanic membrane.

NORMAL EAR

Otoscopic evaluation of a normal ear involves a variety of structures with different tissue types, from external auditory canal skin to the thin translucent tympanic membrane to highly reflective bony ossicles and promontory. The various structures of the middle ear and mastoid have different histological

dx.doi.org/10.1021/ac5030232 | Anal. Chem. 2014, 86, 10454–10460

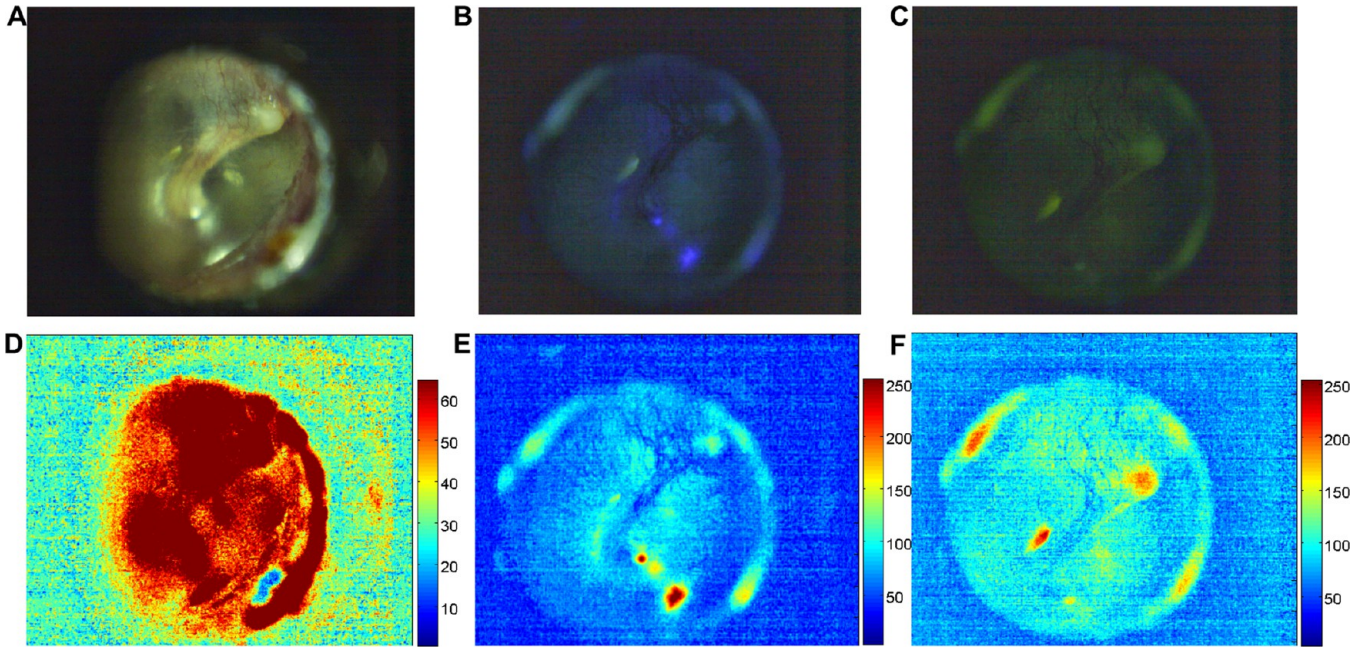

Figure 3. Images of normal tympanic membrane and middle ear using standard white light otoscopy (A) and fluorescence imaging (405 nm excitation (B) and 450 nm excitation (C)). The vascularity along the ear ossicle is well-defined on the white light image. The fluorescence images display very faint signals along the ossicle. Panels D–F represent the contrast-limited adaptive histogram equalization (CLAHE) and denoised counterparts of the raw images (A–C).

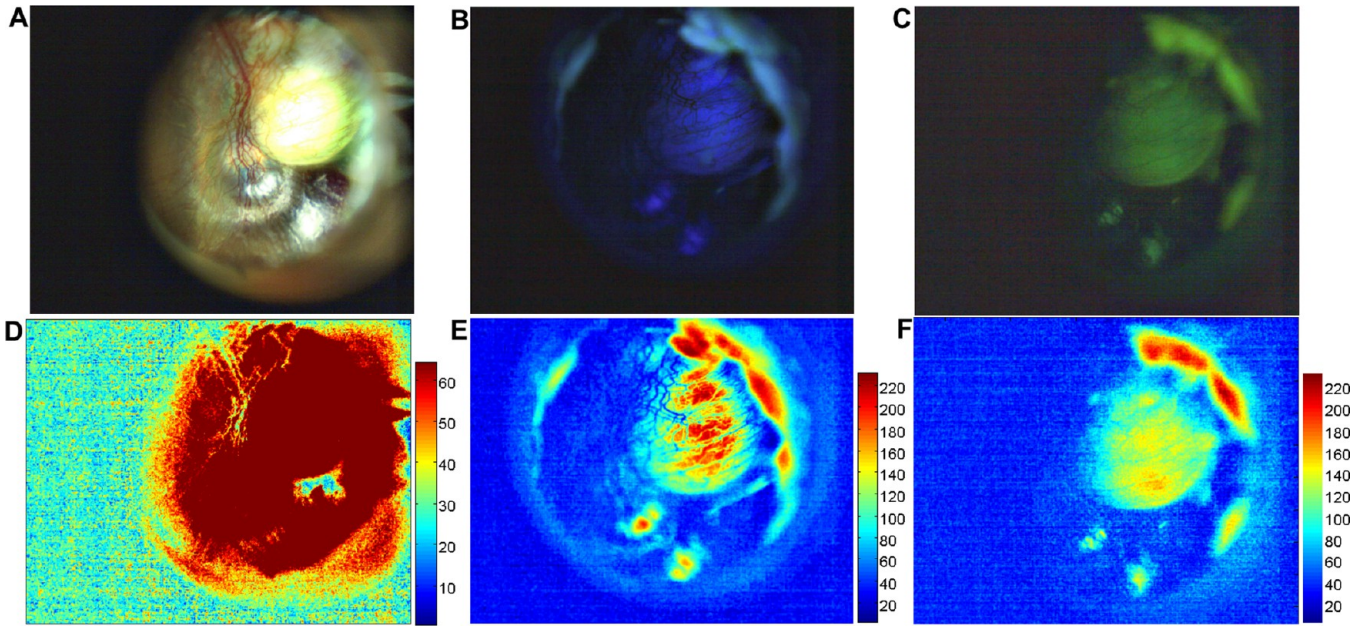

Figure 4. White light (A) and fluorescence images (405 nm excitation (B) and 450 nm excitation (C)) of a congenital cholesteatoma on the superior anterior quadrant of the tympanic membrane. Panels D–F represent the CLAHE and denoised versions of the raw images shown in panels A–C.

compositions and different concentrations of endogenous fluorophores. All these structural variations give specific optical properties that can be potentially targeted using different excitation wavelengths of light.

Figure 3 shows representative images of normal tympanic membrane and middle ear obtained using (A) standard white light otoscopy and fluorescence imaging with (B) 405 nm and (C) 450 nm excitation, respectively. It is evident that the overall intensity of the white light image is (expectedly) much higher than that obtained from autofluorescence. The obtained intensity patterns were quantified and plotted, following adaptive contrast enhancement (Figure 3D–F, in order to better highlight features and margin of the lesion. To obtain the bottom row of figures, contrast-limited adaptive histogram equalization (CLAHE) was performed in Matlab. In contrast to conventional histogram equalization, this algorithm operates on small data regions (tiles) rather than the entire image. Each tile's contrast is enhanced so that the histogram of each output region approximately matches the specified histogram (assumed to be a uniform distribution by default).

The white light image exhibits the cone of light phenomenon, which is commonly observed during examination

dx.doi.org/10.1021/ac5030232 | *Anal. Chem.* 2014, 86, 10454–10460

of the tympanic membrane with an otoscope.[24] This is simply a light reflex event where shining light on the tympanic membrane produces a cone-shaped reflection of light to materialize in the anterior inferior quadrant. Distortions of the cone of light are often used as a marker for increased inner ear pressure. On the other hand, fluorescence imaging with 405 nm excitation and 425 nm emission filter clearly shows that there is no observable signal from the tympanic membrane. However, evidence of fluorescence from the lateral process of the malleus and faint fluorescence from the bony promontory is present. Significant hemoglobin-based absorption is also noticeable, especially in the malleus. Such absorption provides an additional diagnostic marker, but also complicates quantification of the intrinsic fluorescence signal and therefore extraction of direct biochemical information about the identity and concentration of the tissue fluorophores.[25] Autofluorescence in the lateral process of the malleus and promontory is also seen using 450 nm excitation. There was also evidence of a strong fluorescence signal form cerumen in the external auditory canal at both excitation wavelengths.

CONGENITAL CHOLESTEATOMA

In this study, we specifically investigated congential cholesteatomas that are defined as epithelial inclusions behind an intact tympanic membrane in a patient without history of otitis media.[26] Figure 4 displays the white light image and the fluorescence images with 405 and 450 nm excitation acquired from a representative congential cholesteatoma in vivo. The white light image shows the clear presence of a cholesteatoma in the posterosuperior aspect with increased vascularity of the tympanic membrane. Importantly, the cholesteatoma shows a broad fluorescence pattern with evidence of autofluorescence at both 405 and 450 nm excitation. Furthermore, in both the fluorescence images, there is little or no interference from the autofluorescence emitted by the bony promontory and complete absence of autofluorescence from the tympanic membrane. This is promising from a clinical translation standpoint, as the fluorescence images provide clear differentiation between the cholesteatoma and the surrounding uninvolved mucosa. The presence of the cholesteatoma is also unambiguous in the bright field image due to the its highly reflective nature stemming from the large keratin content; however, the presence of the blood vessels and, critically, the boundaries of the lesion are better defined in the autofluorescence images.

An interesting aspect of our observations is the presence of substantive autofluorescence at the two different wavelengths in cholesteatoma. Although the exact origin of these two signals is not known at this time and requires detailed spectroscopic investigations possibly in an in vitro model, one could reasonably infer the contribution of multiple fluorophores to the overall signal levels. Prior reports detail the peak fluorescence emission for keratin at 382 nm with a 50 nm full width at half-maximum for excitation at 277 nm.[27] Thus, the fluorescence signals acquired here would reflect the tail end of the keratin signal with the 405 nm excitation image displaying substantially larger component of the keratin contribution compared to the 450 nm excitation image. Furthermore, Wu et al. have shown that strong keratin fluorescence from the keratinized epithelial layer exhibits similar excitation and emission characteristics to those of collagen.[19] This could also interfere the assessment of NADH/FAD fluorescence in epithelium and collagen fluorescence in stroma, since the former has an optimal excitation in the same wavelength region. This would potentially necessitate the application of multivariate calibration techniques to unscramble the specific contributions in a spectral dataset. Figure 5 shows the H&E stained histologic image of the cholesteatoma, which illustrates the presence and abundance of keratin in this class of hyperproliferative lesions.

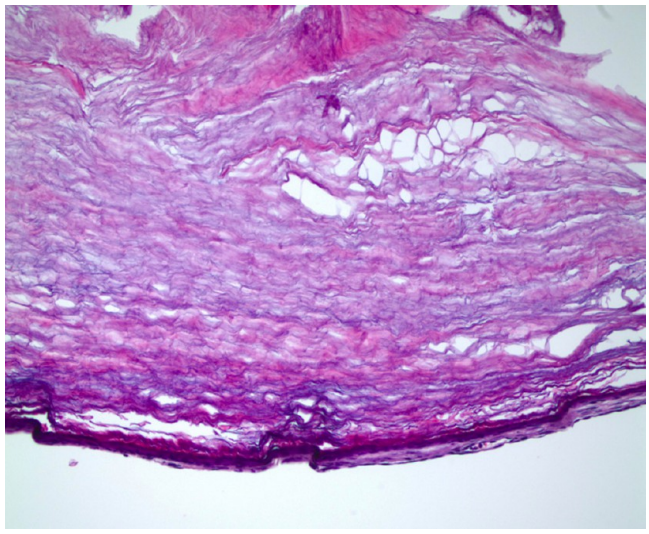

Figure 5. Histologic image of cholesteatoma using H&E stain showing the laminar nature of the keratin in the surface of cholesteatoma resembling the squamous epithelium in the epidermis of skin resting on connective tissue.

DISCUSSION

Standard otoscopic evaluation currently requires subjective visual interpretation of white light reflecting off the tympanic membrane and the middle ear promontory. In other words, the entire process of examining the normal structure, diagnosing diseases and providing critical input for therapy relies extensively on human recognition of morphologic patterns in vivo. This approach is the basis for the current decision-making that has been shown to be less than ideal for a number of conditions, in particular, when it relates to ear examination.[1,2] Specifically, congenital cholesteatomas tend to be asymptomatic until they reach a significant size and rely on an astute clinician to make a diagnosis before the lesion causes significant damage to middle ear structures.[5,28] Detection of congenital cholesteatomas with simple otoscopic examination can be missed altogether or confused with normal conditions such as myringosclerosis. Investigators have opined that even otoscopy with a microscope may not be reliable in predicting the presence or extent of a congenital cholesteatoma.[29]

Through this report, we propose a video-rate, in vivo chemical imaging tool that relies on the differential intrinsic fluorescence signatures observed in tissue and in disease. Our broad hypothesis is spectroscopic measurements of tissue biochemistry represents a measure of objective disease detection and grading that is currently unattainable in clinical practice. In the proof-of-concept studies presented here, the middle ear pathology definition in chemical, rather than morphologic, terms has major implications in the near future. First, the endeavor of lesion margin definition becomes facile and, compared to the existing methods, can improve the quality

of surgical input. Second, it has been hypothesized that biochemical modifications in the margins are precursors of lesion development and growth.[30] Put differently, the morphologically benign-appearing tissue at the margins of proliferative lesions is reported to be biochemically distinct from uninvolved tissue. Identifying molecular targets from this spatial region, then, can establish new opportunities in detection at an early stage and of relapse.

Our data here suggest that different tissue chemical compositions in the tympanic membrane and middle ear provide important information, which is useful in differentiating the cholesteatoma from the normal mucosa at the point of care. We attribute the ability to demarcate the margins to (a) the high keratin content present in cholesteatoma and (b) the metabolic activity in the hyperproliferative lesion. Cholesteatomas have shown a higher apoptotic rate when compared to other external canal cells.[31] This may help explain why cholesteatomas are metabolically more active than the normal tympanic membrane and external auditory canal tissue, resulting in significant NADH/FAD-based autofluorescence. Evidently, determining measurable chemical and metabolic differences between normal and pathologic ear conditions (including inflammatory processes) can help in the development of better diagnostic instrumentation, improving early detection and considerably reducing the number of recurrences following surgery. Our future studies will involve introducing more wavelengths and narrowband filters to improve our diagnostic algorithms to better identify these conditions. Also, time-resolved fluorescence studies may provide vital clues in extricating the precise source of the fluorescence signals, as the NADH/FAD and collagen fluorescence exhibit substantively different time-decay processes.

Additionally, pathologic changes in proliferative lesions in the middle ear such as cholesteatoma require increased vascularization of the surrounding perimatrix to sustain growth.[32] This increase in vascularity was evident due to the ability of hemoglobin to absorb light in this blue-green region of the visible spectrum. We also observed significant fluorescence in cerumen most likely due to the high keratin concentration. Finally, although there was no actual autofluorescence emitted from the tympanic membrane, it allowed fluorescence from the promontory to be captured due to its translucent characteristics. We envision that these properties may be altered in cases of severe inflammation and could be of value in detection of other pathologies such as AOM.

In summary, the nonperturbing nature of this imaging approach is attractive in augmenting otoscopic examination, as is the capability to provide information without the use of contrast agents, which may be ototoxic. Significantly, this imaging modality can be readily adapted to otoendoscopes, which are currently used in otologic surgery to reach difficult access areas intraoperatively.[33]

■ CONCLUSION AND FUTURE PROSPECTS

The present work provides the first report of the design and application of a novel multiwavelength fluorescence-based video otoscope. In this article, we have demonstrated the ability to provide relevant chemical images that map the spatial distribution of important constituents such as collagen, NADH, FAD and keratin. Using congential cholesteatoma detection as a test case, we have shown that the new fluorescence otoscope provides additional information on the proliferative lesion, especially in highlighting its contours and vascularity. This proof-of-concept experiment shows the feasibility of applying the proposed approach for direct in vivo imaging of cholesteatomas in order to aid surgical removal of the lesion, thereby reducing the likelihood of residual disease and improving surgical outcome and patient prognosis. In fact, the presence of residual lesion (which has been reported to be as high as 30%)[4] is widely attributed to be a primary driver of cholesteatoma recidivism.[6]

The results are promising and warrant detailed follow-up investigations. First, the present device prototype only serves to acquire signals from the brightest chromophores and does not provide an adequate signal-to-noise ratio (SNR) for the weakly fluorescent constituents. To overcome this hurdle, the system will have to be redesigned to maximize throughput including installation of a camera with higher quantum efficiency in the UV−visible region. It is worth noting that the SNR drawback of the current system can be partially alleviated by application of denoising algorithms. For example, wavelet-based denoising algorithms have been employed with varying degrees of success by transforming the data in a manner where only a few large (and therefore meaningful) coefficients are retained with the noise being removed by eliminating the smaller wavelet coefficients.[34,35] Also, a larger number of excitation−emission combination wavelengths will have to be studied in order to accurately evaluate their relative diagnostic merit in discerning normal middle ear mucosa from cholesteatoma. It is possible that our current choice of wavelengths, although promising, do not provide optimal performance as far as delineation of proliferative lesions is concerned.

Second, modifications to the current optical design would allow true spectroscopic imaging, i.e., the acquisition of spatial-spectral data cubes where a spectrum is obtained at each uniquely defined spatial point (x, y). Although the current fluorescence imaging dataset has been of value in segmenting lesions from uninvolved tissue, elucidation of the identities and content of the chromophores and/or scatterers would enable true molecular imaging. Multivariate curve resolution of the hyperspectral datasets could provide the spatial distributions of biochemical markers that indicate changes in pathophysiological functions. Additionally, one could envision the use of fluorescence lifetime imaging for otoscopic examination, as it provides an additional dimension of information missing in time-integrated steady-state measurements and is sensitive to biochemical microenvironment. As is well-known, lifetimes (in contrast to direct intensity measurements) are also unaffected by variations in excitation intensity and sources of optical loss and thus may offer a better route to quantification for in vivo measurements. Moreover, the interpretation of the current autofluorescence signals is confounded by the multilayered tissue structure, as the images reflect the volume-averaged contributions of the fluorophores from different tissue layers. A depth-resolved technique, such as confocal fluorescence imaging, would provide a more accurate understanding of the layer-specific fluorescence signals while also avoiding the nonanalyte specific absorption and scattering effects.

From a clinical perspective, the device needs to be prospectively tested in an in vivo clinical study with a substantially larger number of patients and as adjuvant during the surgical procedure. Additionally, other routinely encountered diagnoses, especially acute otitis media (AOM), should be probed in future investigations. AOM represents the most common affliction necessitating medical therapy for children younger than 5 years in the USA and has a significant impact on

the health of children and cost of providing care. We anticipate that the proposed strategy will be sensitive to fluid accumulation, which is a hallmark of AOM. Since most diagnoses made today are of moderate grades with physicians prescribing antibiotics even in the presence of significant diagnostic uncertainty, a tool that can robustly segregate AOM subtypes would be of immense value in routine ENT examination, especially for pediatric cases. Finally, our laboratories have previously employed vibrational spectroscopic methods, namely Raman spectroscopy, for diagnosis of precancerous lesions and cancers in a number of organ systems. By combining the exquisite chemical specificity of Raman spectroscopy with wide-field fluorescence imaging, a multidimensional algorithm capable of differentiating a broader range of middle ear pathologies may be obtained.

AUTHOR INFORMATION

Corresponding Authors

*Tulio A. Valdez, MD. E-mail: tvaldez@connecticutchildrens.org.

*Ishan Barman, PhD. E-mail: ibarman@jhu.edu.

Author Contributions

#These authors contributed equally.

Funding

This research was supported by the Connecticut Institute for Clinical and Translational Science (CICATS), the National Institute of Biomedical Imaging and Bioengineering (9P41EB015871-26A1) and the JHU Whiting School of Engineering Startup Funds.

Notes

The authors declare no competing financial interest.

REFERENCES

(1) Pichichero, M. E. *Eur. J. Clin. Microbiol. Infect. Dis.* **2003**, *22*, 519−524.

(2) Takata, G. S.; Chan, L. S.; Morphew, T.; Mangione-Smith, R.; Morton, S. C.; Shekelle, P. *Pediatrics* **2003**, *112*, 1379−1387.

(3) Rosenfeld, R. M. *Int. J. Pediatr. Otorhinolaryngol.* **2002**, *64*, 89−95.

(4) Sheehy, J. L.; Brackmann, D. E.; Graham, M. D. *Ann. Otol., Rhinol., Laryngol.* **1977**, *86*, 451−462.

(5) Tall, A.; Ba, M. C.; Essalki, I.; Diallo, B. K.; Ndiaye, M.; Loum, B.; Ndiaye, I. C.; Diouf, R.; Diop, E. M. *Dakar Med.* **2006**, *51*, 5−9.

(6) Vartiainen, E. *J. Laryngol. Otol.* **1995**, *109*, 590−592.

(7) Roche, J. P.; Adunka, O. F.; Pillsbury, H. C., 3rd; Buchman, C. A. *Otol. Neurotol.* **2013**, *34*, 1311−1315.

(8) Fernandez, D. C.; Bhargava, R.; Hewitt, S. M.; Levin, I. W. *Nat. Biotechnol.* **2005**, *23*, 469−474.

(9) Bhargava, R.; Fernandez, D. C.; Hewitt, S. M.; Levin, I. W. *Biochim. Biophys. Acta* **2006**, *1758*, 830−845.

(10) Chaiken, J.; Finney, W.; Knudson, P. E.; Weinstock, R. S.; Khan, M.; Bussjager, R. J.; Hagrman, D.; Hagrman, P.; Zhao, Y.; Peterson, C. M.; Peterson, K. *J. Biomed. Optics* **2005**, *10*, 031111.

(11) Breslin, T. M.; Xu, F.; Palmer, G. M.; Zhu, C.; Gilchrist, K. W.; Ramanujam, N. *Ann. Surg. Oncol.* **2004**, *11*, 65−70.

(12) Rajaram, N.; Reichenberg, J. S.; Migden, M. R.; Nguyen, T. H.; Tunnell, J. W. *Lasers Surg. Med.* **2010**, *42*, 716−727.

(13) Draga, R. O.; Grimbergen, M. C.; Vijverberg, P. L.; van Swol, C. F.; Jonges, T. G.; Kummer, J. A.; Ruud Bosch, J. L. *Anal. Chem.* **2010**, *82*, 5993−5999.

(14) Muller, M. G.; Valdez, T. A.; Georgakoudi, I.; Backman, V.; Fuentes, C.; Kabani, S.; Laver, N.; Wang, Z.; Boone, C. W.; Dasari, R. R.; Shapshay, S. M.; Feld, M. S. *Cancer* **2003**, *97*, 1681−1692.

(15) Roblyer, D.; Richards-Kortum, R.; Sokolov, K.; El-Naggar, A. K.; Williams, M. D.; Kurachi, C.; Gillenwater, A. M. *J. Biomed. Opt.* **2008**, *13*, 024019.

(16) Stone, N.; Stavroulaki, P.; Kendall, C.; Birchall, M.; Barr, H. *Laryngoscope* **2000**, *110*, 1756−1763.

(17) Levy, L. L.; Jiang, N.; Smouha, E.; Richards-Kortum, R.; Sikora, A. G. *Laryngoscope* **2013**, *123*, 1016−1020.

(18) Volynskaya, Z.; Haka, A. S.; Bechtel, K. L.; Fitzmaurice, M.; Shenk, R.; Wang, N.; Nazemi, J.; Dasari, R. R.; Feld, M. S. *J. Biomed. Opt.* **2008**, *13*, 024012.

(19) Wu, Y.; Qu, J. Y. *J. Biomed. Opt.* **2006**, *11*, 054023.

(20) Georgakoudi, I.; Jacobson, B. C.; Muller, M. G.; Sheets, E. E.; Badizadegan, K.; Carr-Locke, D. L.; Crum, C. P.; Boone, C. W.; Dasari, R. R.; Van Dam, J.; Feld, M. S. *Cancer Res.* **2002**, *62*, 682−687.

(21) Sokolov, K.; Galvan, J.; Myakov, A.; Lacy, A.; Lotan, R.; Richards-Kortum, R. *J. Biomed. Opt.* **2002**, *7*, 148−156.

(22) Pradhan, A.; Pal, P.; Durocher, G.; Villeneuve, L.; Balassy, A.; Babai, F.; Gaboury, L.; Blanchard, L. *J. Photochem. Photobiol., B* **1995**, *31*, 101−112.

(23) Drezek, R.; Brookner, C.; Pavlova, I.; Boiko, I.; Malpica, A.; Lotan, R.; Follen, M.; Richards-Kortum, R. *Photochem. Photobiol.* **2001**, *73*, 636−641.

(24) Cavanaugh, R. M., Jr. *Pediatrics* **1987**, *79*, 520−523.

(25) Zhang, Q.; Muller, M. G.; Wu, J.; Feld, M. S. *Optics Lett.* **2000**, *25*, 1451−1453.

(26) Derlacki, E. L.; Clemis, J. D. *Ann. Otol., Rhinol., Laryngol.* **1965**, *74*, 706−727.

(27) Pena, A.; Strupler, M.; Boulesteix, T.; Schanne-Klein, M. *Opt. Express* **2005**, *13*, 6268−6274.

(28) Sanna, M.; Zini, C.; Gamoletti, R.; Delogu, P.; Russo, A.; Scandellari, R.; Taibah, A. *J. Laryngol. Otol.* **1987**, *101*, 1221−1226.

(29) Kazahaya, K.; Potsic, W. P. *Curr. Opin. Otolaryngol. Head Neck Surg.* **2004**, *12*, 398−403.

(30) Lieber, C. A.; Nethercott, H. E.; Kabeer, M. H. *Biomed. Opt. Express* **2010**, *1*, 975−982.

(31) Kojima, H.; Tanaka, Y.; Tanaka, T.; Miyazaki, H.; Shiwa, M.; Kamide, Y.; Moriyama, H. *Arch. Otolaryngol., Head Neck Surg.* **1998**, *124*, 261−264.

(32) Fukudome, S.; Wang, C.; Hamajima, Y.; Ye, S.; Zheng, Y.; Narita, N.; Sunaga, H.; Fujieda, S.; Hu, X.; Feng, L.; Lin, J. *JAMA Otolaryngol. Head Neck Surg.* **2013**, *139*, 273−278.

(33) Ayache, S.; Tramier, B.; Strunski, V. *Otol. Neurotol.* **2008**, *29*, 1085−1090.

(34) Donoho, D. L. *IEEE Trans. Inf. Theory* **1995**, *41*, 613−627.

(35) Kwiatkowski, A.; Gnyba, M.; Smulko, J.; Wierzba, P. *Metrol. Meas. Syst.* **2010**, *17*, 549−559.